

Information-Theoretic Gaps in Solar and Reactor Neutrino Oscillation Measurements

Neetu Raj Singh Chundawat^{1, 2, *} and Yu-Feng Li^{1, 3, †}

¹*Institute of High Energy Physics, Chinese Academy of Sciences, Beijing 100049, China*

²*Kaiping Neutrino Research Center, Guangdong 529386, China*

³*School of Physical Sciences, University of Chinese Academy of Sciences, Beijing 100049, China*

Quantum estimation theory provides a fundamental framework for analyzing how precisely physical parameters can be estimated from measurements. Neutrino oscillations are characterized by a set of parameters inferred from experiments conducted in different production and detection environments. The two solar oscillation parameters, Δm_{21}^2 and θ_{12} , can be estimated using both solar neutrino experiments and reactor neutrino experiments. In reactor experiments, neutrinos are detected after coherent vacuum evolution, while solar neutrinos arrive at the detector as incoherent mixtures. In this work, we use Quantum Fisher Information (QFI) to quantify and compare the information content accessible in these two experimental setups. We find that for reactor neutrinos, flavor measurements saturate the QFI bound for both parameters over specific energy ranges, demonstrating their optimality and explaining the high precision achieved by these experiments. In contrast, for solar neutrinos the phase-based contribution to the QFI, originating from the quantum coherence, is absent, rendering the estimation of Δm_{21}^2 purely population-based and effectively classical, while the QFI for θ_{12} is dominated by basis rotation at high energies and is nearly saturated by flavor measurements. Consequently, solar neutrino experiments are intrinsically more sensitive to θ_{12} than to Δm_{21}^2 . This analysis highlights a fundamental distinction between the two estimation problems and accounts for their differing achievable precisions.

I. INTRODUCTION

Quantum mechanics is no longer confined to a fundamental theoretical framework, but also underpins a wide range of modern experimental investigations and technologies. It forms the foundation of the ongoing technological revolution. It is now well established in the literature that, in the noiseless scenarios, quantum properties of systems in consideration can enhance the precision with which parameters governing dynamical processes are estimated. Quantum Estimation Theory (QET), exemplifies how uniquely quantum resources can be exploited to achieve performance beyond classical limits [1].

Estimation theory is a central part of statistics that focuses on how information can be extracted most efficiently from data. In many models, some variables are directly measurable observables, while others are latent parameters that characterize the system but cannot be accessed through direct measurement. In many quantum experiments, the measurement process is inherently destructive, so the system cannot be measured repeatedly. As a result, the repeatability condition of projective measurements is no longer satisfied. A typical example is a photon being absorbed by a polarization filter, after which it is no longer available for further measurements. In such situations, only the probabilities of the measurement outcomes are relevant, while the post-measurement state plays no role. For systems that are measured only once, generalized measurements described by positive operator-valued measures (POVMs) provide the appropriate framework. Mathematically, a POVM consists of a set of non-negative Hermitian

operators acting on the system's Hilbert space, which are not required to be orthogonal or mutually commuting, and which satisfy a completeness relation [2].

The parameter estimation problem concerns how effectively collected data, in the form of observables, can be used to infer unknown latent parameters, and what the best achievable precision is for estimating parameters encoded in a quantum state [3, 4]. By optimizing over all possible POVM measurements, this question is answered by the quantum Cramér-Rao bound (QCRB), which constitutes a central result of QET. The QCRB is determined entirely by the quantum Fisher information (QFI), which depends only on the quantum state. QFI is a central quantity in quantum information theory, with important practical implications in areas such as quantum metrology, where it serves as the quantum analogue of the classical Fisher information (CFI) [5–7].

Neutrino oscillations[8] provide one of the most powerful probes of physics beyond the Standard Model, and achieving increasingly precise determinations of the oscillation parameters has become a primary objective of current neutrino experiments. Neutrino oscillations are characterised by three mixing angles ($\theta_{12}, \theta_{13}, \theta_{23}$), two independent mass-squared differences ($\Delta m_{21}^2, \Delta m_{31}^2$), and a CP-violating phase (δ_{CP}). Among these, solar neutrino experiments predominantly constrain the parameters θ_{12} and Δm_{21}^2 , which are collectively referred to as the solar oscillation parameters[9–11]. These oscillation parameters were independently tested and supported by reactor neutrino measurements with very precise determination of solar mass-squared splitting[12, 13]. Recently, the JUNO reactor neutrino experiment presented its first physics results, demonstrating unprecedented precision in the determination of the solar oscillation parameters[14, 15]. A coordinated global effort combining data from solar, at-

* chundawat@ihep.ac.cn

† liyufeng@ihep.ac.cn

mospheric, reactor, and accelerator neutrino experiments has led to progressively more precise determinations of the parameters governing neutrino oscillations [16].

Solar neutrino experiments and reactor neutrino experiments operate in completely different environments. Solar neutrinos propagate through matter with varying density inside the Sun, then through vacuum, and finally through the matter of the Earth [17–23]. In reactor neutrino experiments, neutrinos propagate essentially in vacuum, with matter effects being present but very small [24, 25]. The agreement between the oscillation parameters Δm_{21}^2 and θ_{12} determined from solar neutrino experiments and reactor neutrino experiments had a number of important implications for neutrino physics. More than two decades later, with more measurements, a difference has emerged between the values of Δm_{21}^2 extracted from solar and reactor neutrino experiments with significance slightly greater than 1.5σ . It may be due to a statistical fluctuation or systematic effects, but it could also turn out to be a manifestation of new physics.

In recent years, there has been growing interest in treating neutrino oscillations as quantum systems within the framework of quantum information science [26–34]. In this work, we study the QFI associated with reactor and solar neutrino oscillations. Since these two systems exhibit qualitatively different quantum properties, it is essential to analyze them within the framework of QET in order to contrast the information encoded in their respective quantum states and assess the effectiveness of different measurement strategies for parameter estimation. We treat both solar neutrino oscillations and reactor neutrino oscillations within an effective two-flavor framework involving only the solar oscillation parameters.

The plan of this work is as follows. In Section II, we introduce the general definitions of the QFI for a generic quantum system. In Section III, we derive the QFI for solar oscillation parameters in the reactor case, followed by the corresponding derivation for solar neutrino oscillations in Section IV. The behavior of these quantities for the KamLAND and JUNO baselines and across the solar neutrino energy range is discussed in Section V. Finally, we present our concluding remarks in Section VI.

II. FISHER INFORMATION

Given a set of measurement outcomes x , an estimator $\hat{\alpha}(x)$ assigns to each outcome an estimate $\alpha = \hat{\alpha}(x)$ of the unknown parameter α . A fundamental result of estimation theory states that the variance of any unbiased estimator is bounded from below by the Cramér–Rao inequality,

$$\text{Var}(\hat{\alpha}) \geq \frac{1}{M F(\alpha)}, \quad (1)$$

where M denotes the number of independent measurements and $F(\alpha)$ is the CFI. For any quantum measurement, the CFI is upper bounded by the QFI, leading

to the quantum Cramér–Rao bound. The QFI depends only on the quantum states of the statistical model and is independent of the specific measurement performed.

The QFI is commonly interpreted as a measure of how much information about an unknown parameter can, in principle, be extracted from a quantum state. It can be defined via the symmetric logarithmic derivative in the eigenbasis of the density operator $\hat{\rho}(\alpha)$ as

$$F_Q^{(S)}(\alpha) = 2 \sum_{j,k} \frac{|\langle \psi_j | (\partial_\alpha \hat{\rho}(\alpha)) | \psi_k \rangle|^2}{p_j + p_k}, \quad (2)$$

where p_i and $|\psi_i\rangle$ denote the eigenvalues and eigenstates of $\hat{\rho}(\alpha)$, respectively.

Since both the eigenvalues and eigenstates may depend on the parameter α , the QFI naturally separates into two distinct contributions, which can be written as

$$F_Q^{(S)}(\alpha) = \sum_i \frac{(\partial_\alpha p_i)^2}{p_i} + 2 \sum_{j \neq k} \frac{(p_k - p_j)^2}{p_j + p_k} |\langle \psi_j | \partial_\alpha \psi_k \rangle|^2. \quad (3)$$

The first term corresponds to the CFI associated with variations of the probability distribution $p_i(\alpha)$, while the second term represents the genuinely quantum contribution arising from parameter-dependent eigenstates. If the eigenstates of $\hat{\rho}(\alpha)$ are independent of θ , the second term vanishes and the QFI reduces to the CFI. In a limited sense, the classical contribution is sensitive only to amplitudes, whereas the quantum contribution encodes information from both amplitudes and phases.

The QFI satisfies several important properties. In particular, it is additive for independent quantum systems. For two independent states $\hat{\rho}_1(\alpha)$ and $\hat{\rho}_2(\alpha)$, the QFI obeys

$$F_Q^{(S)}(\hat{\rho}_1(\alpha) \otimes \hat{\rho}_2(\alpha)) = F_Q^{(S)}(\hat{\rho}_1(\alpha)) + F_Q^{(S)}(\hat{\rho}_2(\alpha)). \quad (4)$$

Another key property of the QFI is convexity with respect to quantum states. For two states $\hat{\rho}_1(\alpha)$ and $\hat{\rho}_2(\alpha)$ prepared with probabilities p_1 and p_2 such that $p_1 + p_2 = 1$, the QFI satisfies

$$F_Q^{(S)}(p_1 \hat{\rho}_1(\alpha) + p_2 \hat{\rho}_2(\alpha)) \leq p_1 F_Q^{(S)}(\hat{\rho}_1(\alpha)) + p_2 F_Q^{(S)}(\hat{\rho}_2(\alpha)). \quad (5)$$

For a pure quantum state $|\psi(\alpha)\rangle$ depending smoothly on the same parameter α , the QFI simplifies to

$$F_Q^{\text{pure}}(\alpha) = 4 \left(\langle \partial_\alpha \psi | \partial_\alpha \psi \rangle - |\langle \psi | \partial_\alpha \psi \rangle|^2 \right), \quad (6)$$

where $|\partial_\alpha \psi\rangle \equiv \frac{\partial}{\partial \alpha} |\psi\rangle$. The above expression is employed for pure-state neutrinos in the subsequent analysis.

III. QUANTUM FISHER INFORMATION OF REACTOR NEUTRINOS

JUNO is an electron antineutrino detector located at an average distance of about 52.5 km from several nuclear

reactors in China. Its excellent energy resolution makes JUNO particularly well suited for precision studies in the neutrino sector [35]. KamLAND is also a medium-baseline reactor experiment in which neutrino oscillations are well described by an effective two-flavour framework, providing a clean measurement of the solar oscillation parameters through vacuum oscillations [12, 13]. For simplicity, we also employ an effective two-flavor framework for JUNO in order to directly compare its results with the KamLAND determination of the solar oscillation parameters, as well as with those obtained from solar neutrino experiments. The corrections from the three-neutrino oscillation framework are subleading and will be relevant for the measurements of Δm_{31}^2 and neutrino mass ordering.

In reactor neutrino experiments, neutrinos propagate coherently over macroscopic baselines in vacuum, and the flavour state remains pure. So, to derive the QFI for these pure state neutrinos, we use Eq. (6). Consequently, the evolved state can be written as

$$|\psi(\theta_{12}, \phi)\rangle = \cos \theta_{12} |\nu_1\rangle + \sin \theta_{12} e^{-i2\phi} |\nu_2\rangle. \quad (7)$$

We can define the standard oscillation phase accumulated during the neutrino propagation as,

$$\phi \equiv \frac{\Delta m_{21}^2 L}{4E} \quad (8)$$

1. QFI for Mixing Angle

Now, to derive the QFI for mixing angle, we take the derivative of the state with respect to θ_{12} and taking the inner product of the derivative, we get

$$\langle \partial_{\theta_{12}} \psi | \partial_{\theta_{12}} \psi \rangle = 1. \quad (9)$$

The overlap between the state and its derivative can be derived as

$$\langle \psi | \partial_{\theta_{12}} \psi \rangle = 0. \quad (10)$$

Using the Eqs. (9) and (10) into the expression for pure state QFI given in Eq. (6), we get,

$$F_Q^\nu(\theta_{12}) = 4. \quad (11)$$

From the above expression, it is evident that the QFI associated with the mixing angle is constant and does not depend on the oscillation phase or the detector baseline. This implies to the maximum amount of information stored in any system about a parameter.

We now compute the Fisher information associated with flavour measurements, since in neutrino oscillation experiments, the oscillation parameters are inferred by flavour dependent observables. Such flavour measurements correspond to projective measurements in flavour space, which can be represented as

$$E_e = |\nu_e\rangle\langle\nu_e|, \quad E_\mu = |\nu_\mu\rangle\langle\nu_\mu|, \quad E_e + E_\mu = \mathbb{I}. \quad (12)$$

The probability to detect an electron neutrino is

$$P_{ee} = 1 - \sin^2(2\theta_{12}) \sin^2(\phi). \quad (13)$$

Since the measurement has two outcomes, the CFI associated with this POVM is

$$F_{\text{flavor}}(\theta_{12}) = \frac{(\partial_\theta P_{ee})^2}{P_{ee}(1 - P_{ee})}. \quad (14)$$

Using Eqs. (13) and (14), we get

$$F_{\text{flavor}}^\nu(\theta_{12}) = \frac{4 \cos^2(2\theta_{12}) \sin^2(\phi)}{1 - \sin^2(2\theta_{12}) \sin^2(\phi)} \quad (15)$$

Hence, from the above expression it is evident that the Fisher information based on flavor POVM satisfies $F_{\text{flavor}}^\nu(\theta_{12}) \leq F_Q^\nu(\theta_{12}) = 4$, where $F_Q^\nu(\theta_{12})$ is the QFI optimized over all POVMs. The bound is saturated at specific values of the oscillation phase ϕ given in Eq. (8).

2. QFI for Mass-Squared Difference

To calculate QFI for Δm_{12}^2 we need to follow the same steps as above. Differentiate Eq. (7) w.r.t. ϕ :

$$\frac{\partial}{\partial \phi} |\psi\rangle = -2i \sin \theta_{12} e^{-i2\phi} |\nu_2\rangle. \quad (16)$$

From the expression in Eq. (6), we can derive the available QFI for the phase as,

$$F_Q^\nu(\phi) = 4 \sin^2(2\theta_{12}). \quad (17)$$

Thus, in order to find the QFI for Δm_{12}^2 we need to use the chain rule for parameters:

$$F_Q^\nu(\Delta m_{21}^2) = F_Q^\nu(\phi) \left(\frac{\partial \phi}{\partial (\Delta m_{21}^2)} \right)^2. \quad (18)$$

Therefore, using this reparameterization, we get the QFI for Δm_{12}^2 as

$$F_Q^\nu(\Delta m_{21}^2) = \sin^2(2\theta_{12}) \left(\frac{L}{2E} \right)^2. \quad (19)$$

Thus, it is evident from the above expression that the QFI for Δm_{12}^2 is energy and baseline dependent.

Following the same approach as for the mixing angle, we compute the Fisher information for flavour measurements for Δm_{12}^2 , and is given as,

$$F_{\text{flavor}}^\nu(\phi) = \frac{4 \sin^2(2\theta_{12}) \cos^2 \phi}{1 - \sin^2(2\theta_{12}) \sin^2 \phi}. \quad (20)$$

Using the chain rule for Δm_{12}^2 similar to as given in Eq. (18) and combining it with Eq. (20) the Fisher information for this POVM can be written as,

$$F_{\text{flavor}}^\nu(\Delta m_{21}^2) = \left(\frac{L}{2E} \right)^2 \frac{\sin^2(2\theta_{12}) \cos^2 \phi}{1 - \sin^2(2\theta_{12}) \sin^2 \phi}. \quad (21)$$

The above expression shows that, analogous to the QFI, the Fisher information based on the flavor measurement depends explicitly on both the propagation length and the neutrino energy.

IV. FISHER INFORMATION OF SOLAR NEUTRINOS

The Sun is a source of electron neutrinos with energies of order MeV, produced through thermonuclear fusion reactions in its core. They allow for direct insight into the interior of the Sun, and their expected production rates are described by the Standard Solar Model (SSM). The SSM brings together the conditions of hydrostatic equilibrium, the mechanisms of energy transport, and the nuclear reactions that are responsible for Solar energy output. When these physical properties are combined with observational constraints such as the radius, age, luminosity, chemical composition, and radiative opacity,

the model provides detailed and consistent predictions for temperature, density, pressure profiles, and neutrino fluxes inside the Sun. Once neutrino oscillation physics is incorporated, the SSM successfully reproduces a broad set of solar observables.

Solar neutrinos are produced incoherently and propagate through regions of high and slowly varying matter density. In this regime, neutrinos follow the instantaneous matter eigenstates, and flavor conversion proceeds via adiabatic Mikheyev-Smirnov-Wolfenstein (MSW) evolution rather than vacuum-like oscillations. At high energies, neutrinos emerge from the Sun predominantly in the ν_2 mass eigenstate, while at lower energies the emerging state is an energy-dependent mixture of ν_1 and ν_2 . In either case, oscillatory interference effects are washed out due to wave-packet separation during propagation from the Sun to Earth [20, 36].

Solar neutrino flavor evolution in the two-flavor approximation framework is described by a Schrödinger-like equation in the flavor space,

$$i \frac{d}{dL} \begin{pmatrix} \nu_e \\ \nu_x \end{pmatrix} = \left[\frac{1}{2E} \begin{pmatrix} \cos \theta_{12} & \sin \theta_{12} \\ -\sin \theta_{12} & \cos \theta_{12} \end{pmatrix} \begin{pmatrix} m_1^2 & 0 \\ 0 & m_2^2 \end{pmatrix} \begin{pmatrix} \cos \theta_{12} & \sin \theta_{12} \\ -\sin \theta_{12} & \cos \theta_{12} \end{pmatrix}^\dagger + \begin{pmatrix} V_e & 0 \\ 0 & 0 \end{pmatrix} \right] \begin{pmatrix} \nu_e \\ \nu_x \end{pmatrix}, \quad (22)$$

where ν_x denotes the non-electron neutrino state, L is the propagation distance, E the neutrino energy, θ_{12} is the mixing angle, and $m_{1,2}$ the neutrino masses. Matter effects are encoded in the effective potential $V_e = \sqrt{2} G_F n_e$, which arises from coherent forward scattering of electrons.

For solar neutrinos, assuming adiabatic propagation in the Sun and neglecting the contribution of the third mass eigenstate, the state can be described as,

$$\rho_\odot(\alpha) = p_1(\alpha) |\nu_1\rangle\langle\nu_1| + p_2(\alpha) |\nu_2\rangle\langle\nu_2|, \quad p_1 + p_2 = 1, \quad (23)$$

where $p_1 = \cos^2 \theta_{12}^m$, $p_2 = \sin^2 \theta_{12}^m$. and the survival probability can be written as

$$P_{ee}^\odot \approx \frac{1}{2} + \frac{1}{2} \cos 2\theta_{12}^m \cos 2\theta_{12}, \quad (24)$$

where the matter-modified mixing angle is given by

$$\cos 2\theta_{12}^m \approx \frac{\cos 2\theta_{12} - \beta_{12}}{\sqrt{(\cos 2\theta_{12} - \beta_{12})^2 + \sin^2 2\theta_{12}}}, \quad (25)$$

and the term β_{12} is given by

$$\beta_{12} \equiv \frac{2V_e^0 E}{\Delta m_{21}^2}. \quad (26)$$

where V_e^0 denotes the value of V_e at the center of the Sun. The three flavor corrections induced by non-zero θ_{13} are neglected and can be found in Ref. [21].

After adiabatic MSW evolution and phase averaging, solar neutrinos arrive at the detector as an incoherent

mixture of mass eigenstates, described by a diagonal density matrix in that basis. In such situations, the second term of Eq. (3) vanishes, and the estimation problem becomes effectively classical. As a result, the QFI reduces exactly to the CFI whenever the eigenvectors of the density matrix does not depend on the parameter under consideration. For mixing angle, the eigenvectors depend on the θ_{12} through mass-flavour basis relation. Therefore, we need to estimate this basis-rotation term in the QFI for mixing angle but this term would not contribute in the Fisher information for mass-squared difference.

We can decompose the QFI given in Eq. (3) in two parts as,

$$F_Q^\odot(\alpha) = F_C^\odot(\alpha) + F_{rot}^\odot(\alpha) \quad (27)$$

where F_C^\odot corresponds to the contribution arising from the eigenvalue populations and therefore coincides with CFI associated with an eigenbasis. The F_{rot}^\odot denotes the contribution due to the parameter dependence of the eigenbasis. For convenience, we also redefine some of the quantities appearing in the probability expression, as

$$\delta \equiv \cos 2\theta_{12} - \beta_{12}, \quad (28)$$

and

$$\Delta_m \equiv \sqrt{\delta^2 + \sin^2 2\theta_{12}}. \quad (29)$$

The matter-mixing in Eq. (25) becomes,

$$\cos 2\theta_{12}^m = \frac{\delta}{\Delta_m} \quad \text{and} \quad \sin 2\theta_{12}^m = \frac{\sin 2\theta_{12}}{\Delta_m}. \quad (30)$$

Using the eigenvalues $\{p_1, p_2\}$, and noting that the normalization condition implies that all information is encoded in p_1 , it is sufficient to compute the Fisher information for this single eigenvalue. We thus obtain a general expression for the CFI with respect to α as

$$F_C^\odot(\alpha) = \frac{\Delta_m^2}{\sin^2 2\theta_{12}} (\partial_\alpha \cos 2\theta_{12}^m)^2. \quad (31)$$

We will now calculate $F_Q^\odot(\alpha)$ for both oscillation parameters for solar neutrino oscillations scenario.

1. QFI for Mixing Angle

We first calculate $F_C^\odot(\theta_{12})$ and by taking the derivative of the matter-mixing term w.r.t. the vacuum mixing angle θ_{12} , we obtain,

$$\partial_{\theta_{12}}(\cos 2\theta_{12}^m) = -\frac{2 \sin 2\theta_{12} (\sin^2 2\theta_{12} + \delta \cos 2\theta_{12})}{\Delta_m^3}. \quad (32)$$

Substituting the above into the general QFI expression given in Eq. (31), we obtain the final expression for population-based term of QFI for mixing angle in solar neutrino case,

$$F_C^\odot(\theta_{12}) = \frac{4 (\sin^2 2\theta_{12} + \delta \cos 2\theta_{12})^2}{\Delta_m^4}. \quad (33)$$

For a two level system, we can write $F_{rot}^\odot(\theta_{12}) = 4(p_1 - p_2)^2$, and for solar case, we obtain it to be,

$$F_{rot}^\odot(\theta_{12}) = 4 \left(\frac{\delta}{\Delta_m} \right)^2. \quad (34)$$

Hence, the total QFI follows from Eq. (3) by inserting Eqs. (33) and (34).

To determine the Fisher information for the flavour measurement schemes, we use the solar survival probability given in Eq. (24),

$$F_{\text{flavor}}^\odot(\alpha) = \frac{(\partial_\alpha P_{ee}^\odot)^2}{P_{ee}^\odot(1 - P_{ee}^\odot)}. \quad (35)$$

In terms of our reddefinition of the parameters, the oscillation probability becomes,

$$P_{ee}^\odot = \frac{1}{2} \left(1 + \cos 2\theta_{12} \frac{\delta}{\Delta_m} \right)$$

and the denominator of Eq. (35) can be written as,

$$P_{ee}^\odot(1 - P_{ee}^\odot) = \frac{1}{4} \frac{\sin^2 2\theta_{12} (1 + \delta^2)}{\Delta_m^2}.$$

Now, to calculate the numerator of the same equation we need to take the derivative of P_{ee}^\odot w.r.t. mixing angle θ_{12} ,

$$\partial_{\theta_{12}} P_{ee} = -\frac{\sin 2\theta_{12} (\delta^3 + \delta + \cos 2\theta_{12} \sin^2 2\theta_{12})}{\Delta_m^3}. \quad (36)$$

Using the evaluated numerator and denominator in Eq. (35), the Fisher information for the flavour POVM is obtained as

$$F_{\text{flavor}}^\odot(\theta_{12}) = \frac{4 (\delta^3 + \delta + \cos 2\theta_{12} \sin^2 2\theta_{12})^2}{(1 + \delta^2) \Delta_m^4}. \quad (37)$$

2. QFI for Mass-Squared Difference

In this case, $F_{\text{rot}}^\odot(\Delta m_{21}^2)$ vanishes, since the eigenbasis does not depend explicitly on the mass-squared difference. Therefore, it is sufficient to evaluate only the population contribution $F_C^\odot(\Delta m_{21}^2)$. To this end, differentiating the matter-mixing term with respect to the parameter β_{12} , we obtain

$$\partial_{\beta_{12}}(\cos 2\theta_m^0) = -\frac{\sin^2 2\theta_{12}}{\Delta_m^3}. \quad (38)$$

Using the above equation in the general form of CFI, we get,

$$F_C^\odot(\beta_{12}) = \frac{\sin^2 2\theta_{12}}{\Delta_m^4}. \quad (39)$$

Using the chain rule to calculate CFI for the solar mass-squared splitting, we obtain the final expression as,

$$F_C^\odot(\Delta m_{21}^2) = \left(\frac{\beta_{12}}{\Delta m_{21}^2} \right)^2 \frac{\sin^2 2\theta_{12}}{\Delta_m^4}. \quad (40)$$

To compute the Fisher information for the flavour POVM with respect to the mass-squared difference using Eq. (35), we first take the derivative with respect to the parameter β_{12} .

$$\partial_{\beta_{12}} P_{ee}^\odot = -\frac{\cos 2\theta_{12} \sin^2 2\theta_{12}}{2 \Delta_m^3} \quad (41)$$

Using the chain rule, we obtain the derivative with respect to the mass-squared difference,

$$\partial_{\Delta m_{21}^2} P_{ee}^\odot = \frac{\cos 2\theta_{12} \sin^2 2\theta_{12}}{2 \Delta_m^3} \frac{\beta_{12}}{\Delta m_{21}^2}. \quad (42)$$

We obtain the Fisher information for the flavour POVM associated with Δm_{21}^2 as

$$F_{\text{flavor}}^\odot(\Delta m_{21}^2) = \left(\frac{\beta_{12}}{\Delta m_{21}^2} \right)^2 \frac{\cos^2 2\theta_{12} \sin^2 2\theta_{12}}{(1 + \delta^2) \Delta_m^4}. \quad (43)$$

V. RESULTS AND DISCUSSIONS

For neutrinos treated as pure states, QFI associated with the mixing angle θ_{12} is constant and equal to 4, whereas the corresponding Fisher information obtained from a flavor POVM exhibits an oscillatory dependence

on the mixing angle and the oscillation phase. In contrast, for the mass-squared parameter Δm_{21}^2 , both the QFI and the flavor-based Fisher information depend non-trivially on the mixing angle and the phase. In this section, we analyze the behaviour of the QFI obtained in the preceding sections for reactor and solar NO.

We take the baseline of JUNO (52.5 km) and KamLAND (180 km) and use the standard values of the relevant oscillation parameters [16]. We plot the quantity η^ν , defined as the ratio of the Fisher information extracted using a flavor POVM to the total QFI available in the state. Here, the ratio η^ν is defined for electron-flavor POVM only. As shown in Fig. 1, this quantity exhibits an oscillatory dependence on the neutrino energy for both oscillation parameters.

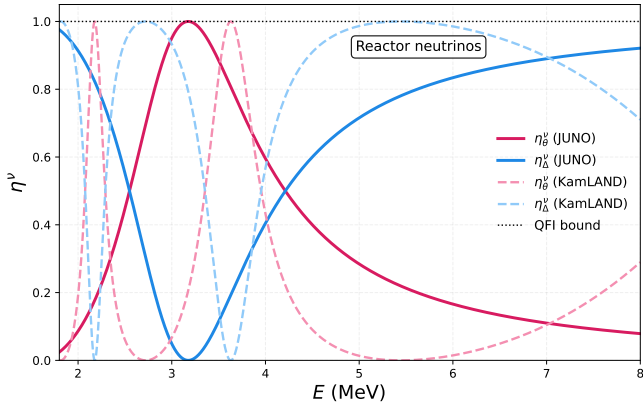


FIG. 1. The extracted fraction η^ν for reactor neutrinos as a function of the neutrino energy E for KamLAND and JUNO baselines. The red solid (dashed) curve corresponds to η^ν for θ_{12} , the blue solid (dashed) curve represents η^ν for Δm_{21}^2 for JUNO (KamLAND), and the black dotted line denotes the quantum limit set by the QFI.

For the mixing angle θ_{12} as can be seen from Fig. 1, the ratio η_θ^ν for KamLAND reaches the QFI bound at certain energies below 4 MeV, indicating that flavor measurements saturate the quantum limit in this energy range. Around 5-6 MeV, the ratio drops close to zero and then starts increasing again at higher energies. This behaviour shows that, while flavor measurements constitute an optimal measurement strategy below 4 MeV, they are unable to extract the available full information around higher energies, and are therefore suboptimal in that region.

For JUNO, the extracted fraction η_θ^ν reaches its maximum around $E \simeq 3$ MeV, exhibiting a broader peak compared to KamLAND. This energy coincides with the mean reactor antineutrino energy and shows that flavour measurements in this region have access to maximum information available on the parameter θ_{12} . At higher energies, η_θ^ν decreases, indicating that JUNO is particularly optimal for estimating θ_{12} in the lower-energy region of the reactor neutrino spectrum. It is to be noted that the corrections from θ_{13} are not taken into account in the current analysis.

For the mass-squared splitting Δm_{21}^2 , the behaviour of η_Δ^ν is similar to that of η_θ^ν below 4 MeV for KamLAND. However, at higher energies the ratio η_Δ^ν remains saturated over a wider energy range, indicating that the flavor POVM continues to extract a significant fraction of the available QFI. This suggests that flavor measurements constitute an effective measurement strategy for estimating Δm_{21}^2 for KamLAND. In addition, as the neutrino propagates, the oscillation phase accumulates, leading to an increase in the information encoded in the quantum state. This accumulation of phase information is also reflected in the energy dependence of the Fisher information shown in the Fig. 1.

In the case of JUNO, the ratio η_Δ^ν exhibits a nontrivial energy dependence. Near the inverse beta decay threshold, η_Δ^ν starts close to unity and decreases to nearly zero around $E \simeq 3$ MeV. Beyond this energy, η_Δ^ν increases again but does not reach the QFI bound up to 8 MeV. Nevertheless, for $E \gtrsim 4$ MeV the extracted fraction remains larger than about 0.5, indicating that a substantial amount of Fisher information is accessible over this energy range. This implies that flavor measurements are suboptimal below ~ 3 MeV and, although not fully optimal at higher energies, they still enable a precise determination of Δm_{21}^2 due to the large fraction of information extracted. Hence, from the perspective of Fisher information, both reactor experiments, KamLAND and JUNO, are capable of estimating the solar oscillation parameters with high precision, and this is also supported by the experimental measurements from both experiments.

Since solar neutrinos constitute a qualitatively different quantum system from an information-theoretic standpoint, we analyze the same set of quantities as in the reactor case using the eigenvalue structure of the density matrix. We separately evaluate the population term and the basis-rotation term for both oscillation parameters, and find that the latter vanishes for the mass-squared difference, reducing the estimation problem to an effectively classical one. For the flavor POVM, the Fisher information is obtained directly from the solar survival probability for both parameters. We organize the discussion into three distinct energy regimes:

- *Low-energy Region:*

In the low-energy limit, where $\beta_{12} \ll 1$, neutrino propagation is vacuum-like and matter effects can be neglected, so that $\theta_{12}^m \rightarrow \theta_{12}$. In this regime, the QFI for θ_{12} attains its maximum value over the entire energy range, as shown by the blue curve in Fig. 2. Using the corresponding low-energy approximation in Eq. (33) and (34), the QFI is found to be close to 4 and decreases monotonically as β_{12} increases. The population contribution, $F_C^\odot(\theta_{12})$, indicated by the orange curve, closely follows the total QFI and therefore dominates the information content in this regime. The dot-dashed black curve shows the electron neutrino survival probability P_{ee}^\odot for reference. The Fisher information associated with the flavor POVM is represented by the green

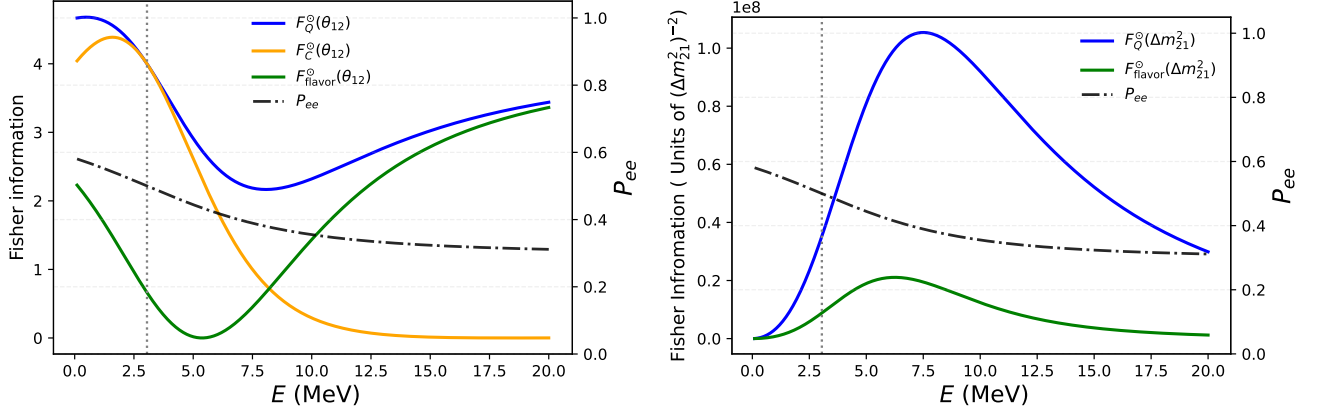


FIG. 2. The left panel shows the Fisher information for θ_{12} , while the right panel corresponds to Δm_{21}^2 as a function of neutrino energy E for solar neutrinos. In the left panel, the blue curve denotes the QFI, the orange curve represents the population contribution, and the green curve shows the Fisher information associated with the flavor POVM. In the right panel, the blue and green curves correspond to the QFI and the flavor POVM Fisher information for Δm_{21}^2 , respectively. The electron-neutrino survival probability P_{ee}^\odot is indicated by the black dot-dashed curve, and the MSW resonance point is marked by the black dotted line.

curve. Since in this limit P_{ee}^\odot depends only on θ_{12} , flavor measurements extract a larger amount of information on this parameter from the total QFI available in the system. This indicates that flavor measurements are suboptimal in the low-energy regime.

In the case of Δm_{21}^2 , basis-rotation contribution vanishes, and the available information arises solely from the population term and the QFI ($F_Q^\odot(\Delta m_{21}^2) \simeq F_C^\odot(\Delta m_{21}^2)$) is negligible at low neutrino energies. As the energy increases, the $F_Q^\odot(\Delta m_{21}^2)$ in the solar neutrino state begins to rise, as shown by the blue curve in Fig. 2. For flavor measurements, the solar survival probability P_{ee}^\odot depends primarily on the mixing angle, and variations in Δm_{21}^2 have little impact on them at low energies. Consequently, the Fisher information associated with the flavor POVM also vanishes in this limit and increases only as the energy grows and the survival probability departs from its vacuum value. In this region, flavor measurements extract a non-negligible fraction of the information on Δm_{21}^2 , however, the total information available in the solar neutrino state remains intrinsically limited.

• MSW Transition Region:

In this energy range, θ_m varies rapidly with energy, approximately over $E \simeq 1\text{-}6$ MeV. As a result, the QFI for θ_{12} decreases sharply from its low-energy value, as shown by the blue curve in Fig. 2, with the population contribution (orange curve) exhibiting the same behavior and providing the dominant contribution. This indicates that the MSW effect does not enhance the information on θ_{12} ; instead, the precision with which the mixing angle can be estimated is reduced in the transition region compared

to the vacuum-dominated regime. For the flavor POVM, the Fisher information (green curve) follows a similar trend but drops to zero in this energy interval, demonstrating that flavor measurements become strongly suboptimal for the determination of θ_{12} within the MSW transition region.

In contrast to θ_{12} , the QFI for Δm_{21}^2 increases in the MSW transition region, since the location of the transition is governed by the mass-squared difference. Consequently, the available information on Δm_{21}^2 is encoded in the energy dependence of the MSW turn-over, corresponding to spectral Fisher information rather than oscillatory phase information. Similarly, the Fisher information associated with the flavor POVM increases in this energy range. However, as shown in the right panel of Fig. 2, it does not saturate the total QFI of the state. This indicates that, although flavor measurements become more informative for Δm_{21}^2 in the MSW region, they remain a suboptimal measurement strategy, with a substantial gap persisting between the accessible information (green curve) and the total information available in the state (blue curve).

• High-Energy Region:

In the matter-dominated regime, where $\beta_{12} \gg 1$, the QFI for θ_{12} increases again. Towards the high-energy end of the spectrum, as P_{ee}^\odot becomes solely a function of θ_{12} , the corresponding QFI approaches values of order 3-4. In this region, the population contribution to the QFI becomes negligible for θ_{12} , while the basis-rotation contribution given in Eq. (34) dominates the total information. The Fisher information associated with the flavor POVM closely follows the QFI and, unlike in the low-energy regime, approaches the maximum information avail-

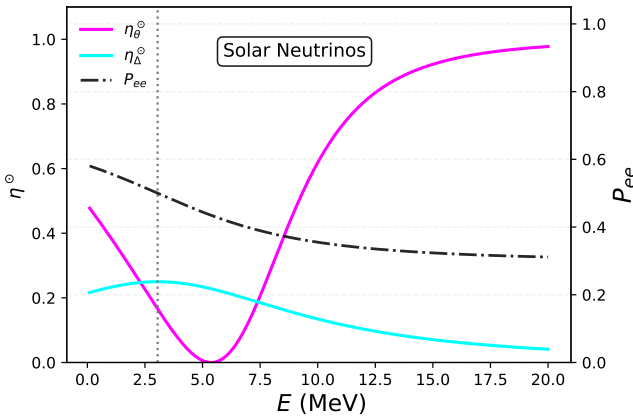


FIG. 3. Extracted fraction η° as a function of the neutrino energy E for solar neutrinos. The magenta and cyan curves correspond to η° for θ_{12} and Δm_{21}^2 , respectively.

able in the state. Consequently, flavor measurements become effectively optimal in the matter-dominated region, nearly saturating the quantum limit.

For the mass-squared difference, the QFI decreases at high energies, with the Fisher information associated with the flavor POVM exhibiting a similar trend. Since P_{ee}° becomes independent of Δm_{21}^2 and depends only on the mixing angle in this regime, the corresponding flavor Fisher information vanishes in the high-energy limit. This demonstrates that flavor measurements are strongly suboptimal for estimating Δm_{21}^2 in the matter-dominated region and are unable to access most of the information available in the quantum state.

We now define a quantity analogous to that introduced for the reactor case, namely the extracted fraction for both oscillation parameters, which quantifies the amount of information accessible through flavor measurements relative to the maximum Fisher information available in the quantum state. This ratio, denoted by η° , characterizes the efficiency of flavor measurements in extracting the available information, and its energy dependence is shown in Fig. 3. It is to be noted, just like in the reactor case, η° is defined for electron-flavor measurements only.

The extracted fraction η_θ° , shown by the magenta curve in Fig. 3, takes relatively large values in the low-energy region and decreases towards zero in the MSW transition region. This indicates that the fraction of the total information on θ_{12} accessible through flavor measurements is significantly higher at low energies than in the MSW region. In the high-energy, matter-dominated regime, η_θ° increases with energy and approaches unity, indicating that flavor measurements nearly saturate the quantum limit and are therefore optimal in this range. Overall, solar experiments employing flavor measurements provide a robust determination of θ_{12} .

As evident from Fig. 3, the extracted fraction η_Δ° for Δm_{21}^2 is of order 0.2 in the low-energy region, increases moderately, and attains a maximum near the MSW resonance. This behavior reflects the fact that variations in the mass-squared difference shift the position of the MSW resonance, thereby enhancing the flavor Fisher information and increasing η_Δ° . At higher energies, η_Δ° decreases significantly and remains at a small but non-vanishing value towards the high-energy end of the spectrum.

Hence, solar experiments exhibit sensitivity to both oscillation parameters, Δm_{21}^2 and θ_{12} , similar to reactor experiments. However, in the solar case, θ_{12} can access the full QFI available in the system. The comparatively weaker determination of Δm_{21}^2 follows naturally from this information-theoretic perspective. In this way, the differing precisions achieved in solar measurements of the oscillation parameters can be consistently understood through the framework of QFI.

VI. CONCLUSION AND OUTLOOKS

In this work, we examined parameter estimation in neutrino oscillation experiments from an information-theoretic perspective. Solar and reactor neutrino experiments both provide precise determinations of the relevant oscillation parameters, albeit with markedly different levels of precision. We address this disparity at a fundamental level by asking whether it is governed by the amount of information encoded in the quantum state at the time of detection for the parameter under consideration. To this end, we employ a central quantity of quantum estimation theory, the Quantum Fisher information (QFI). The QFI can be understood as the classical Fisher information optimized over all possible measurements, reflecting the fact that the accessible information is strongly dependent on the choice of measurement.

As reactor neutrinos propagate coherently over vacuum baselines, the off-diagonal elements of the density matrix survive and contribute to the phase-based QFI. For the mixing angle θ_{12} , the QFI remains constant over the entire energy range, while the Fisher information obtained from a flavor POVM depends on the oscillation phase through the ratio L/E . In contrast, for the mass-squared difference Δm_{21}^2 , both the QFI and the Fisher information associated with the flavor POVM exhibit a nontrivial dependence on L/E . We show that, for both parameters, flavor measurements saturate the maximum QFI available in the quantum state at specific energies, thereby achieving the quantum limit for KamLAND. For JUNO, the QFI bound is saturated for θ_{12} , whereas for Δm_{21}^2 the flavor POVM is able to access a large fraction of the information present in the quantum state over an extended energy range, although it does not fully saturate the quantum limit. This explains the precise determination of the solar oscillation parameters in reactor experiments such as KamLAND and JUNO.

For solar neutrino oscillations, the neutrino state at

detection is an incoherent mixture of mass eigenstates due to the combined effects of production in the solar core, adiabatic MSW evolution, and the long propagation distance between the Sun and the Earth. As a result, the phase-based contribution to the QFI vanishes, since the off-diagonal elements of the density matrix are suppressed. For the mixing angle θ_{12} , both the population term and the basis-rotation term are nonzero, yielding a sizable total QFI in the solar neutrino state. The Fisher information associated with the flavor POVM exhibits a similar qualitative behavior: it approaches the quantum limit at high energies and drops to zero in the vicinity of the MSW transition region.

In contrast, for the mass-squared difference Δm_{21}^2 , the basis-rotation contribution to the QFI vanishes, as this parameter does not affect the eigenbasis of the neutrino state. Consequently, the estimation problem reduces to a purely population-based and becomes effectively classical. The amount of information extracted by flavor measurements remains small across the entire energy range, with a modest peak around the MSW region, indicating that observables in experiment are most sensitive to variations of Δm_{21}^2 in this regime. Overall, this explains why flavor-based measurements allow a more precise determination of θ_{12} than of Δm_{21}^2 in solar neutrino experiments.

We show that, for neutrinos produced and propagated under different physical conditions, such as in reactor and solar environments, the amount of Fisher information available for estimating the same parameter can differ, leading to different achievable precisions. Our analysis

shows that even for the same neutrino state, the information content can differ substantially between different parameters, leading to distinct estimation capabilities. As in the solar neutrino case, flavor measurements are suboptimal for the determination of Δm_{21}^2 but remain effective for estimating θ_{12} . In contrast, for reactor neutrino experiments, flavor measurements are optimal for the determination of both oscillation parameters.

Global fits not only combine different experimental determinations of the same oscillation parameters, but also provide access to complementary quantum information relevant for their estimation. As more experiments are included, this can lead to a more complete extraction of the information available on the oscillation parameters. Investigating the QFI across different experimental setups, as well as in their combination, provides insight into the achievable precision of parameter estimates obtained from measurements and offers a useful framework for experimentalists to assess the robustness of the parameters under consideration. This study can be extended to the three-flavor neutrino oscillation framework and directly connected to investigations of neutrino mass ordering and CP violation within the context of multiparameter estimation theory.

ACKNOWLEDGEMENTS

NRSC would like to thank Luis A. Delgadillo for useful discussions. This work was supported in part by the National Natural Science Foundation of China under grant number 12075255.

[1] C. W. Helstrom, “*Quantum detection and estimation theory*,” *J. Stat. Phys.* **1**, 231–252 (1969) .

[2] M. G. A. Paris, “*Quantum Estimation for Quantum Technology*,” *Int. J. Quant. Inf.* **07**, no. supp01, 125–137 (2009) [arXiv:0804.2981 [quant-ph]].

[3] J. Liu, H. Yuan, X. M. Lu and X. Wang, “*Quantum Fisher information matrix and multiparameter estimation*,” *J. Phys. A* **53**, no.2, 023001 (2020) [arXiv:1907.08037 [quant-ph]].

[4] X. M. Lu, X. Wang and C. P. Sun, “*Quantum Fisher information flow and non-Markovian processes of open systems*,” *Phys. Rev. A* **82**, no.4, 042103 (2010) [arXiv:0912.0587 [quant-ph]].

[5] V. Giovannetti, S. Lloyd and L. Maccone, “*Advances in quantum metrology*,” *Nature Photon.* **5**, 222–229 (2011) [arXiv:1102.2318 [quant-ph]].

[6] F. Albarelli, M. Barbieri, M. G. Genoni and I. Gianani, “*A perspective on multiparameter quantum metrology: From theoretical tools to applications in quantum imaging*,” *Phys. Lett. A* **384**, no.12, 126311 (2020) [arXiv:1911.12067 [quant-ph]].

[7] G. Tóth and I. Apellaniz, “*Quantum metrology from a quantum information science perspective*,” *J. Phys. A* **47**, no.42, 424006 (2014) [arXiv:1405.4878 [quant-ph]].

[8] B. Pontecorvo, “*Neutrino Experiments and the Problem of Conservation of Leptonic Charge*,” *Sov. Phys. JETP* **26**, 984–988 (1968)

[9] Q. R. Ahmad *et al.* [SNO], “*Direct evidence for neutrino flavor transformation from neutral current interactions in the Sudbury Neutrino Observatory*,” *Phys. Rev. Lett.* **89**, 011301 (2002) [arXiv:nucl-ex/0204008 [nucl-ex]].

[10] J. P. Cravens *et al.* [Super-Kamiokande], “*Solar neutrino measurements in Super-Kamiokande-II*,” *Phys. Rev. D* **78**, 032002 (2008) [arXiv:0803.4312 [hep-ex]].

[11] G. Bellini *et al.* [Borexino], “*First evidence of pep solar neutrinos by direct detection in Borexino*,” *Phys. Rev. Lett.* **108**, 051302 (2012) [arXiv:1110.3230 [hep-ex]].

[12] T. Araki *et al.* [KamLAND], “*Measurement of neutrino oscillation with KamLAND: Evidence of spectral distortion*,” *Phys. Rev. Lett.* **94**, 081801 (2005) [arXiv:hep-ex/0406035 [hep-ex]].

[13] S. Abe *et al.* [KamLAND], “*Precision Measurement of Neutrino Oscillation Parameters with KamLAND*,” *Phys. Rev. Lett.* **100**, 221803 (2008) [arXiv:0801.4589 [hep-ex]].

[14] A. Abusleme *et al.* [JUNO], “*First measurement of reactor neutrino oscillations at JUNO*,” [arXiv:2511.14593 [hep-ex]].

[15] A. Abusleme *et al.* [JUNO], “*Initial performance results of the JUNO detector*,” [arXiv:2511.14590 [hep-ex]].

[16] I. Esteban, M. C. Gonzalez-Garcia, M. Maltoni, I. Martinez-Soler, J. P. Pinheiro and T. Schwetz, “*NuFit-6.0: updated global analysis of three-flavor neutrino oscillations*”

tions,” JHEP **12**, 216 (2024) [arXiv:2410.05380 [hep-ph]].

[17] S. P. Mikheyev and A. Y. Smirnov, “*Resonance Amplification of Oscillations in Matter and Spectroscopy of Solar Neutrinos,*” Sov. J. Nucl. Phys. **42**, 913-917 (1985)

[18] R. Davis, Jr., D. S. Harmer and K. C. Hoffman, “*Search for neutrinos from the sun,*” Phys. Rev. Lett. **20**, 1205-1209 (1968)

[19] L. Wolfenstein, “*Neutrino Oscillations in Matter,*” Phys. Rev. D **17**, 2369-2374 (1978)

[20] A. Y. Smirnov, “*Solar neutrinos: Oscillations or No-oscillations?,*” [arXiv:1609.02386 [hep-ph]].

[21] X. J. Xu, Z. Wang and S. Chen, “*Solar neutrino physics,*” Prog. Part. Nucl. Phys. **131**, 104043 (2023) [arXiv:2209.14832 [hep-ph]].

[22] G. D. O. Gann, K. Zuber, D. Bemmerer and A. Serenelli, “*The Future of Solar Neutrinos,*” Ann. Rev. Nucl. Part. Sci. **71**, 491-528 (2021) [arXiv:2107.08613 [hep-ph]].

[23] M. Maltoni and A. Y. Smirnov, “*Solar neutrinos and neutrino physics,*” Eur. Phys. J. A **52**, no.4, 87 (2016) [arXiv:1507.05287 [hep-ph]].

[24] Y. F. Li, A. Wang, Y. Xu and J. y. Zhu, “*Terrestrial Matter Effects on Reactor Antineutrino Oscillations: Constant vs. Fluctuated Density Profiles,*” [arXiv:2511.15702 [hep-ph]].

[25] Y. F. Li, Y. Wang and Z. z. Xing, “*Terrestrial matter effects on reactor antineutrino oscillations at JUNO or RENO-50: how small is small?,*” Chin. Phys. C **40**, no.9, 091001 (2016) [arXiv:1605.00900 [hep-ph]].

[26] M. Blasone, S. De Siena and C. Matrella, “*Wave packet approach to quantum correlations in neutrino oscillations,*” Eur. Phys. J. C **81**, no.7, 660 (2021) [arXiv:2104.03166 [quant-ph]].

[27] M. Blasone, F. Dell’Anno, S. De Siena and F. Illuminati, “*Entanglement in neutrino oscillations,*” EPL **85**, 50002 (2009) [arXiv:0707.4476 [hep-ph]].

[28] A. K. Alok, T. J. Chall, N. R. S. Chundawat and Y. F. Li, “*Quantifying Imaginarity in Neutrino Systems,*” [arXiv:2412.01871 [hep-ph]].

[29] K. Dixit, J. Naikoo, S. Banerjee and A. K. Alok, “*Quantum correlations and the neutrino mass degeneracy problem,*” Eur. Phys. J. C **78**, no.11, 914 (2018) [arXiv:1807.01546 [hep-ph]].

[30] A. K. Alok, M. Blasone, T. J. Chall, N. R. S. Chundawat and G. Lambiase, “*Coherent dynamics of flavor mode entangled neutrinos,*” [arXiv:2501.06311 [hep-ph]].

[31] E. C. Nogueira, G. de Souza, A. D. Varizi and M. D. Sam-paio, “*Quantum estimation in neutrino oscillations,*” Int. J. Quant. Inf. **15**, no.06, 1750045 (2017) [arXiv:1610.05388 [quant-ph]].

[32] K. El Bouzaidi, A. Slaoui, L. B. Drissi, E. H. Saidi and R. A. Laamara, “*Dynamics of quantum information resources in two-flavor neutrino oscillations,*” Eur. Phys. J. C **85**, no.11, 1349 (2025)

[33] M. Ignoti, C. Fruguele, M. G. A. Paris and M. G. Genoni, “*Is the large uncertainty of δ_{CP} fundamentally encoded in the neutrino quantum state?,*” [arXiv:2511.20148 [hep-ph]].

[34] B. Yadav, A. Subba and Y. Shi, “*Quantum Fisher Information Revealing Parameter Sensitivity in Long-Baseline Neutrino Experiments,*” [arXiv:2602.05221 [hep-ph]].

[35] F. An *et al.* [JUNO], “*Neutrino Physics with JUNO,*” J. Phys. G **43**, no.3, 030401 (2016) [arXiv:1507.05613 [physics.ins-det]].

[36] E. K. Akhmedov and J. Kopp, “*Neutrino Oscillations: Quantum Mechanics vs. Quantum Field Theory,*” JHEP **04**, 008 (2010) [erratum: JHEP **10**, 052 (2013)] [arXiv:1001.4815 [hep-ph]].